Use of satellite radiance data in the global meteorological model of the German Weather Service (DWD)

D. Pingel

July 23, 2010

Contents

Abstract

As many other weather centers, the German Weather Service (Deutscher Wetterdienst, DWD) uses observations of satellite sounding instruments for the purpose of numerical weather prediction. This is achieved by assimilation of the observational data into the meteorological model in the analysis step of the forecast cycle.

For the DWD global model, this is accomplished by direct assimilation of radiances within a three-dimensional variational physical space analysis scheme. At present, AMSU-A data over sea from NOAA-15, NOAA-18,

NOAA-19 and METOP-2 are assimilated. Preparations for the assimilation of AMSU-B and IASI data into the global modelare currently under way, and first results are to be expected soon. This paper intends to overview the present state of the assimilation of satellite radiance observations in the global model of the DWD and to review an assimilation impact study done with IASI level 2 temperature and humidity retrievals.

1 Operational assimilation of remote sensing data in the global model GME

1.1 The 3D-Var assimilation system at the DWD

The DWD uses the Global MEteorological model (GME) for the numerical weather prediction (NWP) on the global scale. The GME is a hydrostatic model based on an icosahedral horizontal grid. It provides global NWP forecasts and provides boundary and initial conditions for the local model COSMO. In the current version, the GME has a horizontal resolution of 30 km. Vertically, it is composed of 60 layers, reaching up to 5 hPa (sigma hybrid coordinates).
The NWP model is corrected by observational information in the data assimilation step, resulting in the analysis. For the GME, for data assimilation a three-dimensional variational (3D-Var) is used. Observational ($\mathbf{y}$) and GME model background ($\mathbf{x}_b$) information is combined in a statistically optimal way, taking into account background ($\mathbf{B}$) and observation error ($\mathbf{R}$) covariance matrices. A cost function

$$J(\mathbf{x}) = J_o(\mathbf{x}) + J_b(\mathbf{x}) = (H(\mathbf{x}) - \mathbf{y})^T \mathbf{R}^{-1} (H(\mathbf{x}) - \mathbf{y}) + (\mathbf{x} - \mathbf{x}_b)^T \mathbf{B}^{-1} (\mathbf{x} - \mathbf{x}_b)$$

is minimized to yield the analysis $\mathbf{x}$. The minimization is done in observation space (physical space assimilation system, PSAS) to reduce the dimensionality of the numerical problem. A combination of conjugate gradient and Newton method is used to solve the minimization problem, accounting for nonlinearity in the forward operator $H(\mathbf{x})$. The global analysis is calculated eight times daily, with a 3h assimilation time window.

1.2 Satellite data operationally assimilated in the GME

- AMSU/MHS: Currently, AMSU-A radiances from NOAA-15, -18, -19 and Metop-A are operationally assimilated (cloud free FOVs of upper-air channels only, thinned to 240 km horizontal distance). Work on assimilation of AMSU-B/MHS is on the way.

- IASI: Assimilation of IASI radiances is under development. At present, the cloud detection scheme is being tuned for use in the 3D-Var (scheme according to: A.P.McNally, P.D.Watts: A cloud detection algorithm for high- spectral-resolution infrared sounders, Q.J.R. Meteorol. Soc. 129, p. 3411, 2003) [1]

- Atmospheric motion vectors (AMV): AMV data of the geostationary satellites GOES 11 and 12, Meteosat 8 and 9 and MTSAT-1 are assimilated, together with AMV data from the polar orbiting satellites TERRA, AQUA

(both MODIS instruments), NOAA 16-18 and Metop-A (AVHRR instruments).

- Scatterometer: Currently, scatterometer data from ASCAT onboard Metop-A is assimilated.
- GPS radio occultation: Assimilation of radio occultation data of the COSMIC satellites and Metop-A (GRAS instrument) is done operationally.

2 Impact study: Assimilation of geopotential layer thickness observations derived from IASI level 2 retrievals within the 3D-Var

2.1 IASI instrument

The Infrared Atmospheric Sounding Interferometer (IASI) on-board Metop-A is a Fourier transform spectrometer, providing infrared spectra with high resolution between 645 and 2760 cm-1 (3.6 m to 15.5 m). The IASI mission is designed to measure atmospheric emission spectra in order to derive temperature and humidity profiles with high vertical resolution and accuracy. In addition to this, IASI observations allow the determination of trace gases such as ozone, carbon dioxide, methane, and nitrous oxide. Other parameters to be derived from IASI radiances are cloud properties as well as land- and sea surface temperature and emissivity.

2.2 Observations

IASI Level 2 products are disseminated since 25 September 2007. At the DWD, the level 2 product product containing temperature, atmospheric water vapour and surface skin temperature (product code 'TWT') is received as a BUFR file via GTS. The vertical sampling of temperature and humidity is at 90 pressure levels, with a horizontal sampling of about 25 km at nadir. The vertical profiles are retrieved from the IASI L1C data. The IASI Level 2 product makes use not only of the IASI Level 1c radiance spectra but also of measurements of the ATOVS instruments on-board Metop. The data included in the preprocessing of the IASI level 2 data are IASI L1c, AMSU-A L1b, AVHRR L1B, MHS L1b and ATOVS L2 products. Aside from these observational data, NWP data is made use of.
The BUFR data file also contains a number of flag and code tables, giving additional information on metadata and the pre-processing (see Appendix, section **??**). These flags contained in the BUFR data is a sub-set of the processing flags discussed in the following two subsections 2.2.1 and 2.2.2.

2.2.1 IASI Level 2 preprocessing at EUMETSAT

For each individual IASI IFOV, the geolocation is extracted from L1C data (validity indicated by the flag FLG_IASIBAD). A Land-Sea database and a Digital Elevation Model provides the topography and surface type (land/water) for each IFOV (validity indicated by the flag FLG_LANSEA). After performing a valid-bounds check (using NWP data), ATOVS Level 2, AMSU Level 1, MHS Level 1

and AVHRR cloud mask and surface (or cloud top temperature) measurements S/CTT are collocated with the IASI IFOV (result flags FLG_ATOVINT and FLG_AVHAVL). The resulting product allows for the calculation the weighted fractional cloud cover and the weighted S/CTT distributions for the individual IASI IFOV (FLG_IASICLR as output). The NWP forecast data are interpolated on to the position of the IASI IFOV (results in FLG_NWPBAD).

2.2.2 IASI Level 2 retrieval at EUMETSAT

The first retrieval is performed either with IASI alone or IASI in combination with ATOVS data. The numerical method underlying the retrieval is either EOF (Empirical Orthogonal Function) regression or neural network algorithms. The flag FLG_FINCHC indicates which method has been applied. Quality checks of the retrieved humidity (super-saturation) and temperature (super-adiabaticity: output flag FLG_SUPSAT) follow. If necessary, a subsequent iterative retrieval is appended: It is performed by composing a appropriate background state vector from the first retrieval (flag FLG_SELBAC contains the composition of the background state vector). With this background vector and its inverse covariance matrix as input (augmented by climatology), a Fast Radiative Transfer Model calculates synthetic IASI brightness temperature spectra, along with the Jacobians. The state vector then undergoes a series of iterations and calculations of new brightness temperature spectra and Jacobians, while minimising a cost function. Once an acceptable solution is found, the flags FLG_ITCONV, FLG_NUMIT, and FLG_RESID are set, containing information about the convergence of the iteration, number of iterations, and residuals, respectively. In a final quality check, the alignment of the results with the EURD requirements is tested (flag FLG_QUAL).
The iterative retrieval can be applied to individual channels as well as to super channel clusters. Super channel cluster consist of linear combinations of IASI channels, which have highly correlated radiances and therefore contain redundant information.
For further details of the IASI level 2 processing, see [2] and [3], the latter reference also shows some results of an assimilation study using IASI level 2 data.

2.3 Derivation of layer thickness from IASI l2 data

The IASI level 2 data set contains Temperature $T(p_i)$ and humidity mixing ratio $m(p_i)$ on 90 fixed pressure levels p_i. The humidity mixing ratio is supposed to be close to the value of the specific humidity, $m(p_i) \approx q(p_i)$, which is used in the following. In order to simplify the calculation, virtual temperature is derived from temperature and humidity:

$$T_v(p_i) = T_v[T(p_i), q(p_i)] = T(p_i)[1 + q(p_i)(\frac{R_{wv}}{R} - 1)] \tag{1}$$

with the specific gas constant of dry air and water vapour, $R = 287.05\frac{J}{kg\ K}$ and $R_{wv} = 461.51\frac{J}{kg\ K}$, respectively. This allows the use of the barometric height relation:

$$\frac{dp}{p} = -\frac{gdz}{RT_v(p)} \tag{2}$$

and according the ideal gas law

$$p = \rho R T_v(p) \tag{3}$$

it yields

$$-\frac{1}{g}\frac{RT_v(p)}{p}dp = -\frac{\rho^{-1}}{g}dp = dz \tag{4}$$

with the inverse density ρ^{-1}.
The calculation of the geopotential layer thickness is done by integrating the geopotential as derived from the virtual temperature at each pressure level p_i according to eqn. (4).
Seven geopotential layers with boundary pressure values P_j of 1000, 700, 500, 100, 50, 30, 10, and 0 hPa are defined. In former studies, this partitioning has been found to be a good compromise for allowing enough vertical degrees of freedom on the one hand and for reducing the vertical correlations by having not too many levels on the other hand [4]. It had also been in use for the assimilation of satellite retrievals into the former operational assimilation scheme of the DWD, based on optimum interpolation.
The layer thicknesses of the seven layers is calculated as follows: Integration of eqn. (4) in each thickness layer j with boundaries at pressure levels P_j and P_{j+1} (at geopotential heights z_j and z_{j+1}) yields the layer thickness Δz:

$$-\frac{1}{g}\int_{P_j}^{P_{j+1}} \frac{RT_v(p)}{p}dp = \int_{z_j}^{z_{j+1}} dz = (z_{j+1} - z_j) \tag{5}$$

As the virtual temperature profile is discretely sampled, the integral on the left hand side of equation has to be interpolated. Three ways of possible interpolations of the integrand in eqn (5), which corresponds to the inverse value of the density, ρ^{-1}, have been implemented: An interpolation as a step function, an interpolation assuming a linear dependence of the virtual temperature between the sampling pressure levels, and a spline interpolation of the profile (see fig. 1). The interpolation of the integrand done, the integration is then done analytically according eqn. (5). A comparison of the three interpolation methods with first guess layer thicknesses derived from GME model fields within the 3D-Var showed that the interpolation of ρ^{-1} as a linear function seems to be best in terms of innovation statistics. The interpolation as a step function (which corresponds to the calculation of the average ρ^{-1} in each sample layer) has generally larger deviances in all thickness layers. The spline interpolation has results comparable to the linear interpolation in the inner thickness layers, but has larger observation-first guess differences in the topmost and bottommost thickness layer. Therefore, the linear interpolation method of (5) is used in the impact experiments. The nominal observation error correlations for clear and cloudy layer thickness observations (Tab. 1 and 2) are set according to Tab. 4 in [4] and have also been applied in the IO of the DWD, as have been the nominal observation errors (Tab. 3). (The errors differ from the values given in [4] in being slightly larger.)

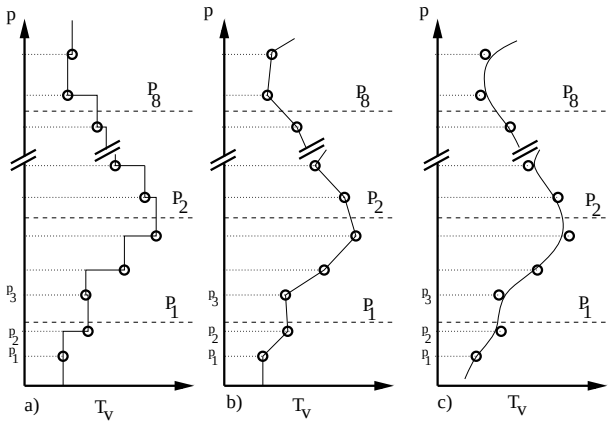

Figure 1: Sketch of geopotential layer thickness interpolation schemes: The inverse density approximated as a (a) step like function, (b) linearly interpolated, and (c) spline interpolated.

Layer (hPa)	1000-700	700-500	500-300	300-100	100-50	50-30	30-10
1000-700	1.00						
700-500	0.22	1.00					
500-300	-0.18	0.27	1.00				
300-100	0.00	0.00	-0.16	1.00			
100-50	0.00	0.00	0.16	0.00	1.00		
50-30	0.00	0.00	0.00	0.15	0.00	1.00	
30-10	0.00	0.00	0.00	0.00	0.00	0.27	1.00

Table 1: Nominal vertical error correlations for **clear** layer thickness observations.

Layer (hPa)	1000-700	700-500	500-300	300-100	100-50	50-30	30-10
1000-700	1.00						
700-500	0.22	1.00					
500-300	-0.34	0.22	1.00				
300-100	0.00	-0.25	-0.29	1.00			
100-50	0.00	0.00	0.00	0.00	1.00		
50-30	0.00	0.00	0.00	0.20	0.00	1.00	
30-10	0.00	0.00	0.00	0.00	0.00	0.27	1.00

Table 2: Nominal vertical error correlations for **cloudy** layer thickness observations

Layer (hPa)	clear		cloudy	
(hPa)	(m)	(K)	(m)	(K)
1000-700	27.0	2.56	33.0	3.13
700-500	17.0	1.72	20.0	2.02
500-300	25.0	1.65	31.0	2.05
300-100	53.0	1.64	56.0	1.74
100-50	33.0	1.62	33.0	1.62
50-30	36.0	2.38	36.0	2.38
30-10	74.0	2.29	74.0	2.29

Table 3: Nominal vertical observation errors for layer thickness observations

Exp.	content
control	no IASI observation data
1	IASI level 2 retrieval data, assimilated as layer thickness, over sea and land
2	as experiment 1, but IASI observations over land and over sea-ice are excluded.

Table 4: Experiments performed to study the influence of IASI level 2 observations on the NWP.

2.4 Experiments

To evaluate the possible impact of the IASI temperature and humidity retrievals, assimilated as layer thicknesses, on the numerical weather forecast, experiments are performed in the numerical experimental suite NUMEX of the DWD (see Tab. 4). The assimilation in the global model GME is done within the operational three-dimensional assimilation system 3D-Var of the DWD, using an observation time window of three hours. The January 2009 is chosen as time period of the experiment. The setup of the 3D-Var and the selection of observations to be assimilated beside the IASI data is as in July 2008. Observation data contain SYNOP, TEMP, PILOT, BUOY, AIREP and AMSU-A radiance observations. In the control experiment, no IASI retrieval observations are assimilated. Layer thickness observations derived from IASI retrievals are assimilated in the experiments 1 and 2. They are assimilated only for cloud-free spots. The cloud information is read from the flag FLG_CLDFRM in the IASI level 2 data set. A horizontal thinning to 55 km ($ni = 128$) is applied to the IASI radiances in the preprocessing step, which removes approximately half of the observations. The remaining amount of layer thickness observations roughly equals the amount of AIREP observation data. In the experiment 1 IASI retrievals over land, sea and sea-ice are used, whereas in experiment 2 only IASI observations over sea are assimilated.

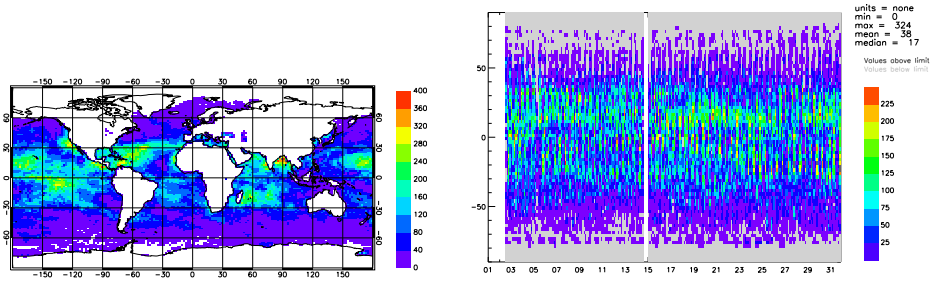

Figure 2: Number of clear sky IASI retrieval observations in the time of the experimental period in January 2009. Box size in the horizontal plot (left) is 2x2 degree. The Hovmoeller diagram (right) shows the observation count for each latitude (2.5 degrees) for each three-hourly assimilation time window.

2.4.1 Monitoring of incoming observational data

The temporal and horizontal distribution of clear sky IASI retrievals over the time of January 2009 is displayed in fig. 2. Within the period of the experiment, no IASI retrieval data are available before 2.1.2009, 12 UTC and at the 14.1.2009, at 15, 18 and 21 UTC. Due to higher cloud-contamination, the mid-latitudes have a lower observation count than the tropics. Areas of remarkably high numbers of received IASI retrievals are west of India the western Carribean sea. However, a part of the differences in observation count in different latitudes visible in fig. 2 is due to the equirectangular projection.
As the layer thicknesses derived from the IASI retrievals are concerned, for all height levels a strong dependence of their value on the latitude can be observed, related to the meridional dependence of the average air mass temperature.
The layer thicknesses values, when monitored over the time of the experimental period, display a trend in the second half of January 2009 in the upper troposphere/lower stratosphere: The IASI retrieval tend to lower temperatures (i.e. smaller values of layer thickness) in the tropics, and to higher temperatures in the areas north of 50 degree latitude, see fig. 3.
The time series in fig. 4 show that these trends are supported by the first guess and, consequently, by the analysis itself. The statistics of the differences observation-first guess and the analysis departures show no significant temporal changes within the one-month period of the experiment. The trend visible in the IASI retrieval therefore can be trusted to reflect a real meteorological process.
A striking feature is the high horizontal variability of the averaged observational values in the northern Atlantic above 300 hPa (see fig. 5 top). Correspondingly, the standard deviation of the observations shows higher values in this region when compared with adjacent areas, see fig. 5 bottom. This feature is visible up to the height of 10 hPa. Time- series monitoring of the north pole region (latitude in [60,90]) suggest that the large values of the observations standard deviation seem to occur predominantly in the first half of the month (see fig. 6). Possible explanation for this feature could be an incorrect ice mask, as the observations are close to the ice edge as given by the ice mask in use.

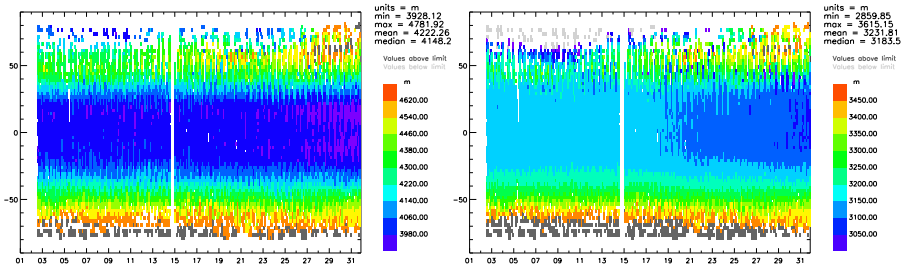

Figure 3: Hovmoeller time-latitude plots of zonally averaged geopotential layer thickness [m] for the layer thickness level 50-100 hPa and 30-50 hPa. Box size is 2.5 degree x 3h.

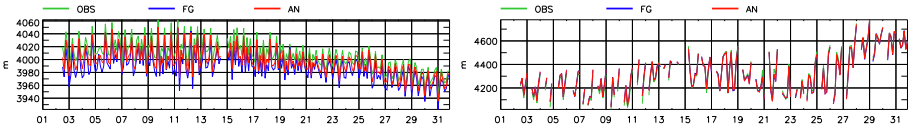

Figure 4: Time series of averaged observational (green), first guess (blue), and analysis (red) values of layer thickness level 50-100 hPa. Considered are the tropics with latitudes in [-20,20] (left) and the north pole region with latitudes in [60,90] (right).

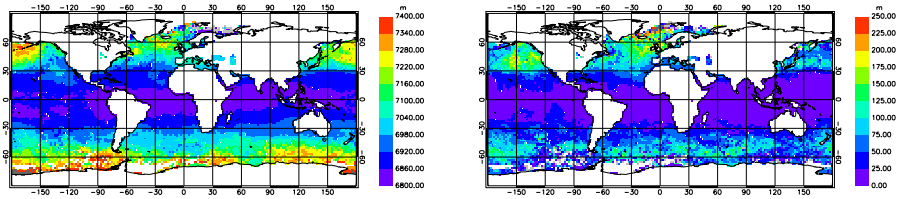

Figure 5: Left: Geopotential layer thickness of the the layer 300-100 hPa, in meter. The observational values show a high horizontal variability in the northern Atlantic. This enhanced variability corresponds to higher values of the standard deviation of the observations (right).

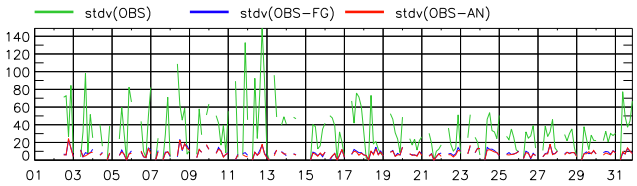

Figure 6: The time series of the standard deviation of the observations in the north polar region suggests that the enlarged variation seems to be generated mainly in the first half of the experimental period.

2.4.2 Analysis differences of IASI experiments 1 and 2 versus control

A snapshot of the atmospheric fields of the three experiments, taken on the 5th day, 00 UTC of the experiment, displays an interesting feature that arises with the assimilation of the IASI retrievals in form of layer thickness observations. In fig. 7, height-latitude plots show the zonal averages of the differences of the analysed fields in the experiments with IASI observations versus the control experiment. Considered fields are geopotential, temperature and relative humidity. The strong influence of IASI observations over land are clearly visible, especially in the polar regions (experiment 1, left colum in fig. 7).
But even when only sea observations are considered, a strong, vertically oscillating temperature bias of up to 1 K builds up against the control, as can clearly be seen in the tropics and mid-latitude. It is positive in the lowest part up to 750 hPa, negative in the adjacent level up to 400 hPa, then again positive up to 200 hPa, and negative above. Vertical structure resembles the thickness layer levels, though it is not identical. However, it is likely that this structure has its origin in the use of thickness layers rather than assimilating smoother retrieval profiles. When assimilating thickness layers, the analysis increments are spread more or less uniformly over an atmospheric layer without accounting for its interior vertical fine structure. Probably a latitude-depending bias correction of the layer thicknesses can be an advantage for the assimilation.
The geopotential field shows a similar vertical pattern (top row of fig. 7. Different to the temperature field, where the negative and positive extreme values equal, the overall geopotential differences seem to be shifted to the negative by approximately 25 m. This is consistent with the innovation statistics of the complete experimental period, fig. 8, displaying a pronounced negative bias in the tropics up to 100 hPa.
A strongly negative bias can be seen in the relative humidity field as seen in the bottom row in fig. 7. The bias is located in the tropics and the lower latitudes with its extreme value of approximately 15 % at a height of 700 hPa and reaches up to a height of 300 hPa. The extreme value is only slightly less pronounced in the experiment with assimilation of IASI retrievals over sea only. The position of the extrema of the bias coincides with the height at which the temperature bias changes from being positive to negative (bottom to top). Therefore it is most probable that the thermal instability induced by the temperature bias results in enhances convection. This in turn results in a increase of precipitation and therefore in a loss of humidity in the height of 700 hPa.
The significant drift in the temperature field that builds up as IASI retrievals are assimilated regardless of the surface type leeds to the conclusion that these retrievals over land and sea-ice are better to be excluded from the observational data set to be assimilated. Thus, the discussion in the following focuses on results of the experiment 2, where only IASI retrievals over sea are assimilated. It is possible that a bias-correction depending on the latitude may cope with the biases impressed onto the temperature field and improve the result of the assimilation, see also [3].

2.4.3 IASI geopotential layer thickness innovation statistics

The statistics of the innovations (differences of observation-first guess) of the geopotential layer thickness observations, derived from the IASI level 2 re-

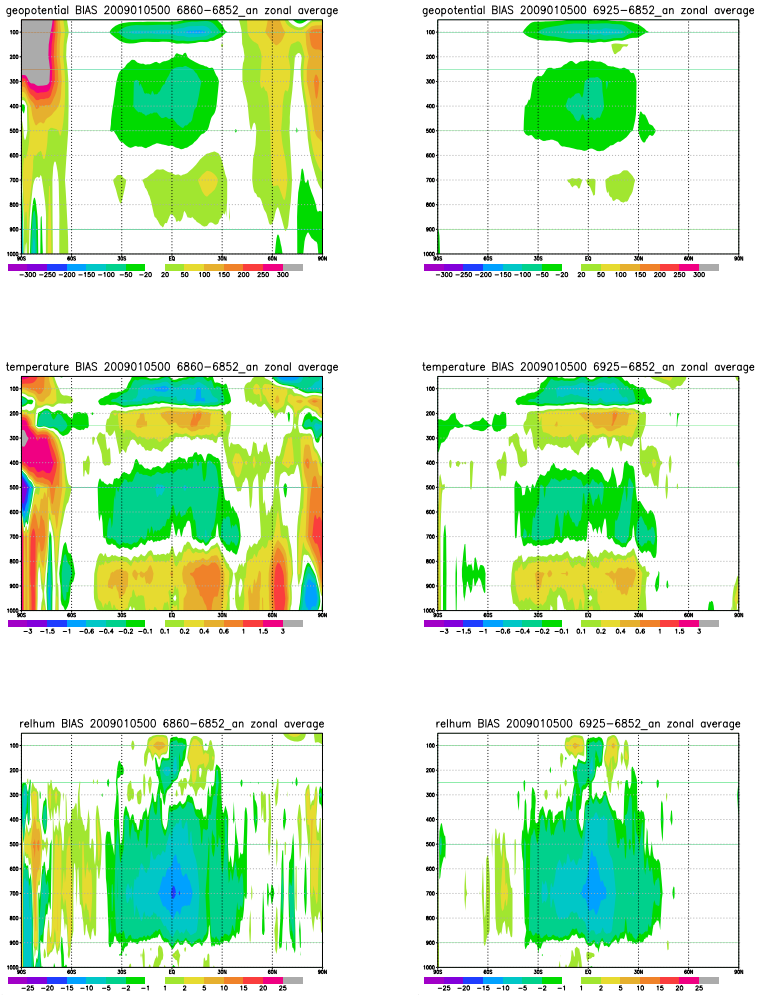

Figure 7: Height-latitude plots of the zonally averaged differences of the analysed fields in the experiments 1 (left) and 2 (right) with IASI observations versus the control experiment. Displayed are geopotential (top), temperature (middle) and relative humidity (bottom).

trievals, is shown in for the northern and southern hemisphere, the tropics and Europe in fig. 8 and for the polar regions in fig. 9. For all latitudes and below the height of 50 hPa, the bias of the IASI observations seems to be confined to ± 20 m and less. For higher levels, a strong positive bias builds up, most probably due to the different use of climatologies in the retrieval algorithm and the GME model. The absolute bias is generally less than 5 m in the lowest layer thickness level (1000-700 hPa), in the southern hemisphere even up to a height of 200 hPa. This is presumably due to the lack of other observations in this area. The three columns in the centre of the figs. 8 and 9 give, for each level, the number of IASI retrievals entering (blue) and exiting (pink) the 3D-Var assimilation. Their respective difference (red) relates to the selective activity of the variational quality control within the 3D-Var. In all areas and height levels, the number of IASI retrieval observations, the absolute value of the bias and the standard deviation is reduced by the application of the variational quality control, as one would expect. The tropical region (fig. 8, second row) is remarkable in that it shows a relatively strong negative bias of approximately 10 m from the lowest level up to a height of 100 hPa. In other latitudes, the negative bias is less pronounced in value and vertical extension. The reason for this feature might be related to the occurrence of vertical structures in the tropical temperature field (as seen in fig. 7) and demands further investigation. Another interesting detail is that in the lowest thickness level in the tropics, the analysed value is warmer than the first guess, whereas the observed value is cooler. A reason for this might be the influence of other observation systems, especially surface measurements. This finding is remarkable as the tropical temperature field in the lower troposphere suffers from a positive bias when IASI observations are included (see fig. 7). The positive bias might at least partially be supported by this feature of the assimilation.

2.5 Radiosonde statistics in IASI and control experiment

The (observation - first guess) bias and standard deviation of radiosonde observation over land and sea for the IASI experiment and the control are considered. Radiosonde observations can be utilised to compare the background fields of temperature and humidity. Figs. 10 to 15 show the radiosonde (observation-first guess) temperature and relative humidity statistics of the experiment with (pink) and without (blue) assimilation of IASI retrievals for the northern (figs. 10 and 11) and southern (figs. 12 and 13) hemisphere and the tropics (figs. 14 and 15) . As the observations are the same in both experiments, a higher (lower) value of the innovations in the IASI experiment, compared to the control, corresponds to a lower (higher) value of the temperature or humidity as a result of the assimilated IASI observations.
In each figure, the top row show the statistics of the radiosondes over land, the bottom row holds the corresponding diagrams for radiosondes located in the sea. In all areas, the impact of the assimilation of IASI retrievals is more pronounced over sea than over land. This is related to the fact that only IASI retrievals over sea are assimilated. Although the global air masses mix within the month of the experiment, this effect is visible. The standard deviation is generally not significantly changed by assimilation of the IASI retrievals (this might confirm the assumption that the IASI retrievals mainly impose a bias to the temperature field, and less noise).

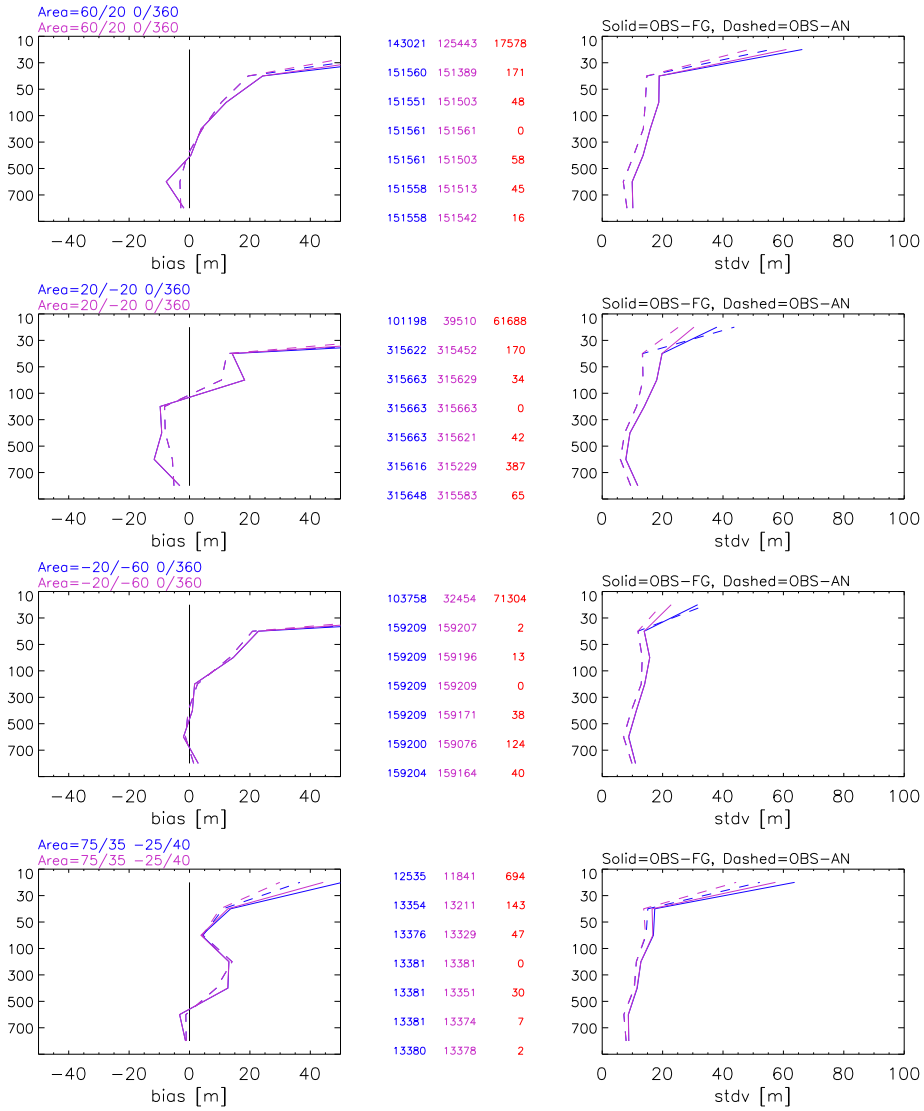

Figure 8: Innovation statistics of IASI retrievals as geopotential layer thicknesses: Bias (left) and standard deviation (right) of observation-first (solid line) and observation-analysis (dashed line) of the experiment with assimilation of IASI retrievals. The statistics of all observations is marked blue, whereas the used observations are marked in pink. The statistics is shown for northern hemisphere, tropics, southern hemisphere and Europe (from top to bottom).

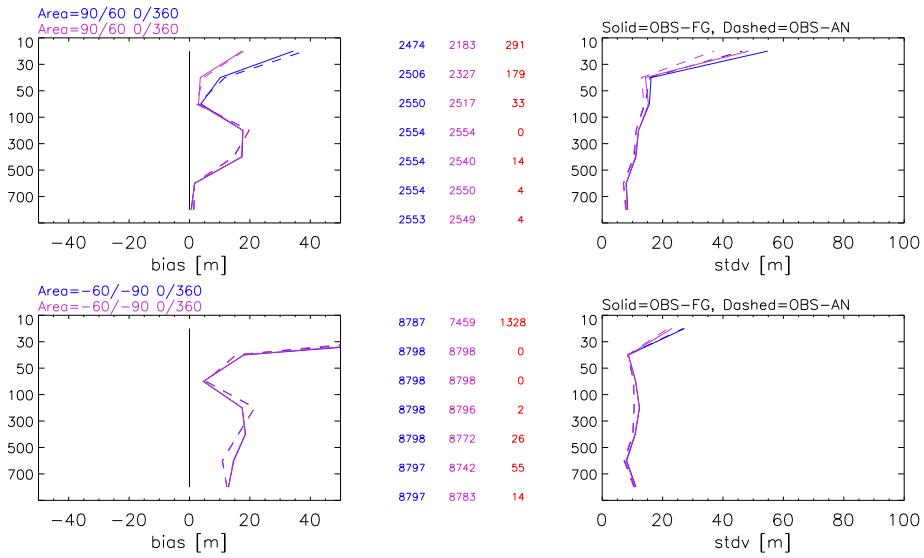

Figure 9: As fig. 8, but for north pole (top) and south pole (bottom).

For the temperature in the tropics, a vertically oscillating pattern can be recognised (fig. 14) : The assimilation of IASI retrieval results in a warming of the atmosphere in the lower troposphere and between the pressure levels of 300 and 150 hPa, 70 and 40 hPa, and above 20 hPa. The atmosphere between these layers with positive temperature increment is cooled relative to the control experiment. The difference in the temperature field have an absolute value of up to 0.3 K. This pattern in the monthly mean value corresponds to the impression given by the vertical section of the zonally averaged temperature field at the day five of the experiment fig. 7. The pattern of the vertical variation of the temperature bias corresponds roughly, but not exactly, the pressure level sequence of the geopotential thickness layers (the most noticeable exception is the subdivision of the layer with negative temperature bias between 700 and 250 hPa into two geopotential thickness layers). This vertically oscillating pattern can, even though less pronounced, be noticed in the southern hemisphere (fig. 12). In contrast, the radiosonde temperature innovations in the northern hemisphere (fig. 10) and in Europe (not shown) show no significant differences for the experiment with and without IASI retrievals.
The differences in the humidity field as to be derived from the radiosonde statistics are a decrease of humidity in the tropical mid-troposphere between 900 and 300 hPa (fig. 15). To a lesser extent this decrease is also visible in the radiosonde innovation statistics of the northern (11) and southern hemisphere (13). It may be pointed out that, according to the radiosonde statistics, the background model seem to be too wet (the bias of (obs-fg) is generally negative), thus the assimilation of IASI retrievals tends to improve the humidity field. The pattern of the tropical relative humidity field again corresponds to the zonally averaged vertical cut through the atmosphere at the fifth day of the experiment fig. 7. The loss of humidity in the middle troposphere is presumably due to the thermal instability introduced by the temperature increment: As the humid tropical air

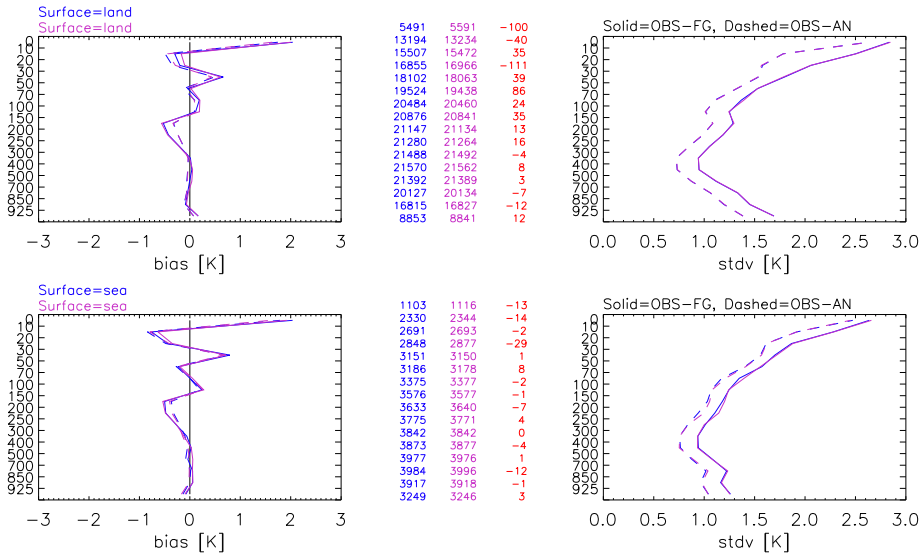

Figure 10: Northern hemisphere radiosonde temperature innovation statistics: Bias (left) and standard deviation (right) of observation-first (solid line) and observation-analysis (dashed line) of the experiment with assimilation of IASI retrievals (pink) and the control experiment (blue). The statistics is shown for land (top) and for sea (bottom) observations.

is heated in the lower troposphere and cooled in the vertically adjacent layer above, convection and precipitation are enhanced. As an effect, the humidity decreases in the mid-troposphere.
The three columns in the centre of each of the figs. 10 to 16 give, for each level, the number of radiosonde observations in the control experiment (blue), in the experiment with IASI retrievals (pink) and their respective difference (red). The radiosonde innovation statistics figs. 10 to 15 indicate that assimilation IASI retrievals reduce the number of radiosondes in the assimilation to some extent. This is a result of a gradual change in the model background fields, which seem to partly drift away from the values of the radiosonde observations. It is interesting that this is not the case for air plane (AIREP) observations in the tropics (fig. 16). For nearly all height levels, more AIREP observations are assimilated in the IASI retrieval experiment than in the control experiment. In addition, for height levels above 800 hPa, the bias of the AIREP innovations is significantly reduced. Also for higher latitudes more AIREP observations are assimilated in the IASI experiment compared to the control, but the influence of IASI observations on the bias of the innovations is less than in the tropics.

2.6 Analysis differences to IFS

To get an impression on the analysed fields within the experiments and the control, their differences to the corresponding fields of the IFS analysis system of the ECMWF as a reference are statistically inspected.
The differences between the control experiment and the operational GME visible for the last few days in figs. 17 to 20 might be related to the switch-off of NOAA

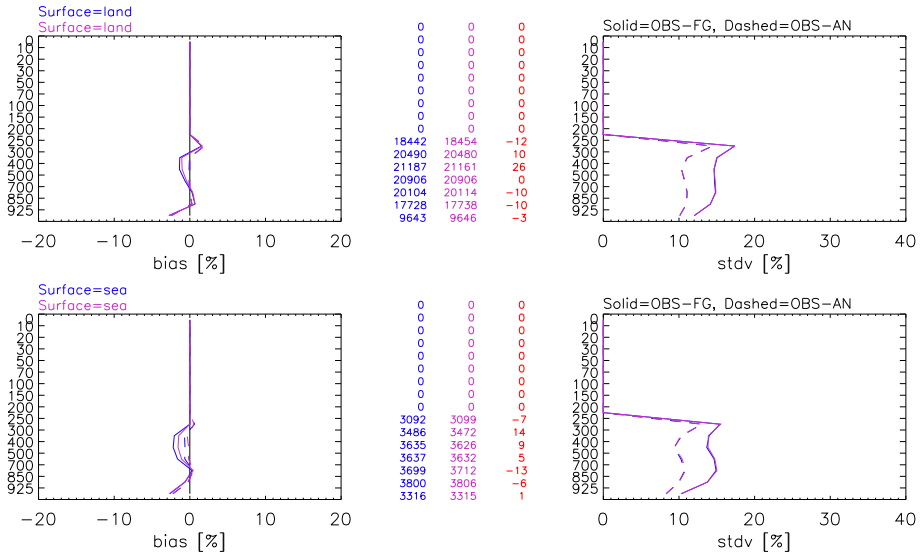

Figure 11: Northern hemisphere radiosonde relative humidity innovation statistics: Bias (left) and standard deviation (right) of observation-first (solid line) and observation-analysis (dashed line) of the experiment with assimilation of IASI retrievals (pink) and the control experiment (blue). The statistics is shown for land (top) and for sea (bottom) observations.

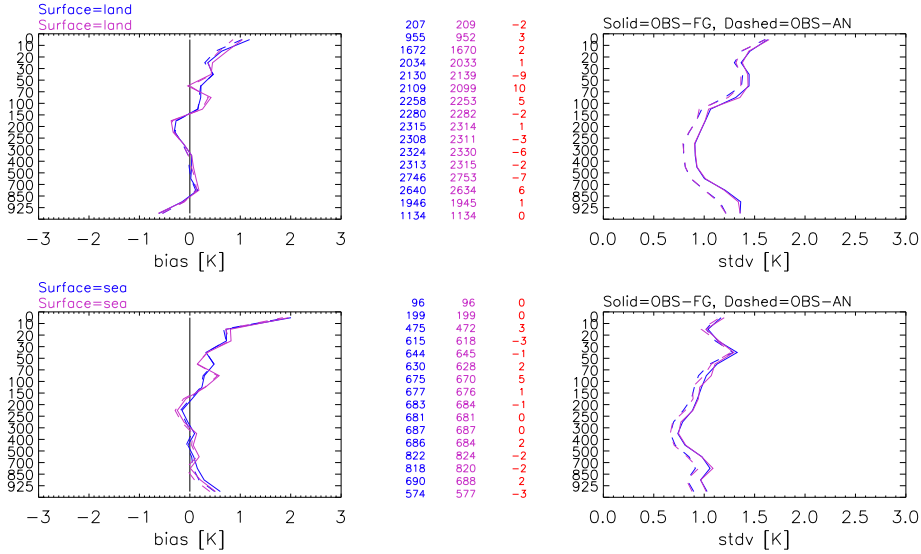

Figure 12: Southern hemisphere radiosonde temperature innovation statistics: Bias (left) and standard deviation (right) of observation-first (solid line) and observation-analysis (dashed line) of the experiment with assimilation of IASI retrievals (pink) and the control experiment (blue). The statistics is shown for land (top) and for sea (bottom) observations.

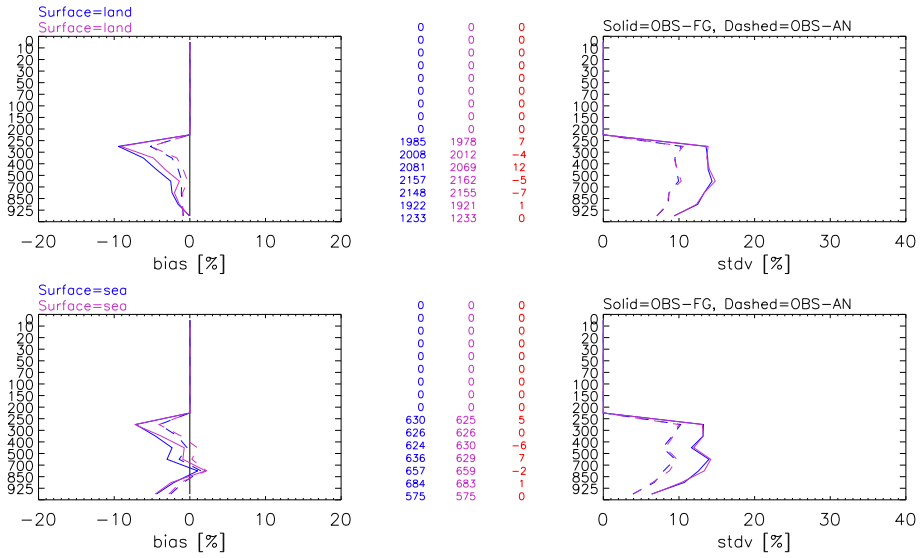

Figure 13: Southern hemisphere radiosonde relative humidity innovation statistics: Bias (left) and standard deviation (right) of observation-first (solid line) and observation-analysis (dashed line) of the experiment with assimilation of IASI retrievals (pink) and the control experiment (blue). The statistics is shown for land (top) and for sea (bottom) observations.

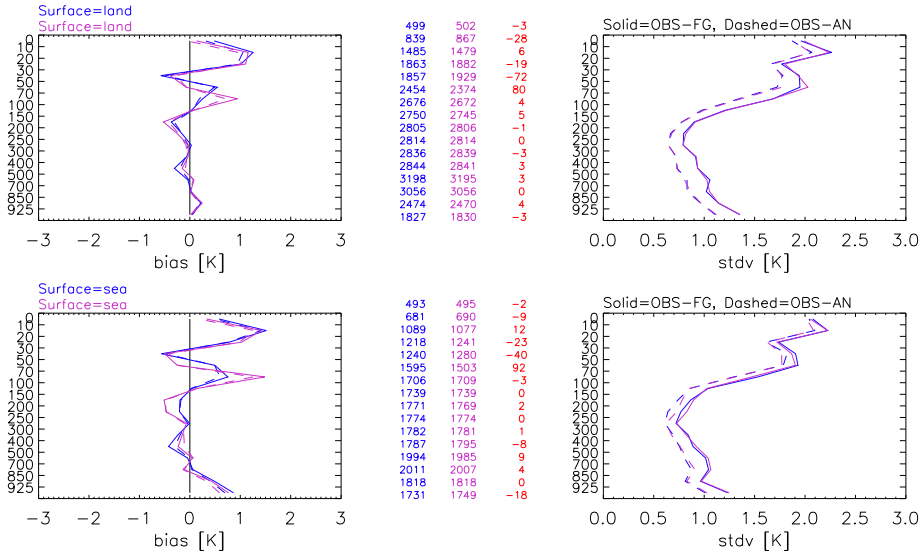

Figure 14: Tropical radiosonde temperature innovation statistics: monthly mean (left) and standard deviation (right) of the observation-background (solid line) and the analysis-background (dashed line) differences. Shown are the statistics for land (top) and sea (bottom) observations. In pink the experiment with assimilation of IASI retrievals, in blue the control experiment.

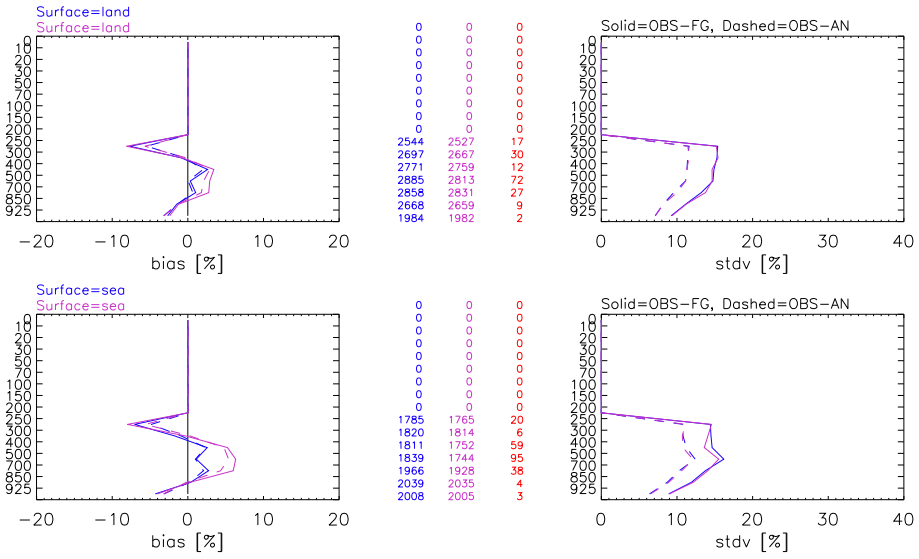

Figure 15: Radiosonde relative humidity innovation statistics for the tropical region: monthly mean (left) and standard deviation (right) of the observation-background (solid line) and the analysis-background (dashed line) differences. Shown are the statistics for land (top) and sea (bottom) observations. In pink the experiment with assimilation of IASI retrievals, in blue the control experiment.

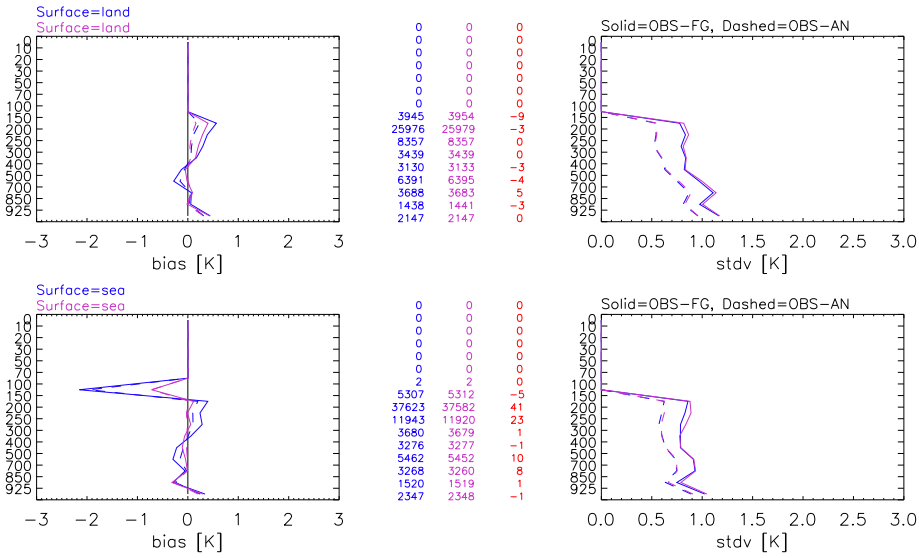

Figure 16: Air plane temperature innovation statistics for the tropical region: monthly mean (left) and standard deviation (right) of the observation-background (solid line) and the analysis-background differences (dashed line). Shown are the statistics for land (top) and sea (bottom) observations. In pink the experiment with assimilation of IASI retrievals, in blue the control experiment.

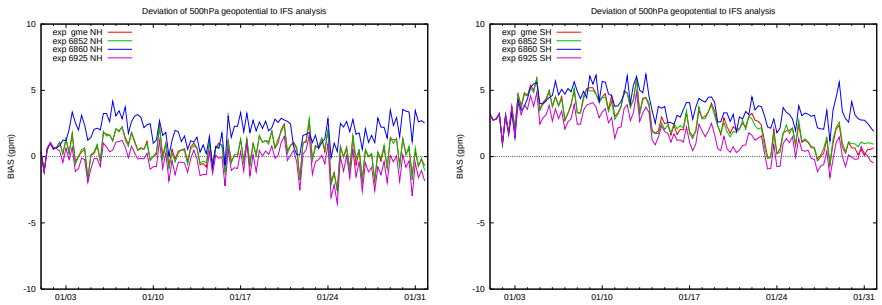

Figure 17: Comparison of the geopotential field at 500 hPa with IFS in the extratropics: Time series of the bias of analysis deviances of assimilation experiments w.r.t. IFS in northern (left) and southern (right) hemisphere. Displayed are: Assimilation of IASI retrievals over sea only (pink), IASI retrievals over land and sea (blue), control experiment (green) and the operational assimilation of the GME (red)

16 at the 28.1.2009 in the operational routine, which had not been taken into account in the experiment.
In the northern and southern hemisphere, the bias of the geopotential field at 500 hPa of experiment 2 with assimilation of IASI retrievals only over sea is slightly better than the control experiment (fig. 17). If IASI land observations are included, like in experiment 1, the bias is increased. Although a quantity not to be trusted to much, the geopotential at 500 hPa in the tropics is significantly closer to the IFS analysis than the control (fig. 18). No significant differences between control and IASI experiments can be noticed when comparing the deviances of the 1000 hPa geopotential fields to the IFS analysis.
The bias of the tropical temperature fields at 850, 500 and 250 hPa with respect to the corresponding IFS fields is enhanced significantly when IASI retrievals are assimilated, see fig 19. The bias is slightly smaller if only IASI observations over sea are considered as in experiment 2. The bias is positive at 850 and 250 hPa and negative at 500 hPa, with a absolute value of approximately 0.5 K. This coincides with the conclusions to be drawn from the radiosonde statistics (fig. 14) and the direct comparison of the two IASI experiments with the control experiment 7. For the temperature in the higher latitudes and for all pressure levels included in the evaluation, the IASI observations have only a minor effect on the analysis differences, also the RMS is not significantly changed (not shown).
As the relative humidity in the tropics is concerned, a large negative bias and an enhanced RMS in comparison with the IFS is introduced by the IASI retrievals (fig. 20). This applies for the height levels 500, 700 and 850 hPa and for both experiments with assimilation of IASI observations. This is consistent with the pattern in the relative humidity field as seen in figs. 15 and 7. In the northern and southern hemisphere, however, no significant differences are found in comparison with the control.

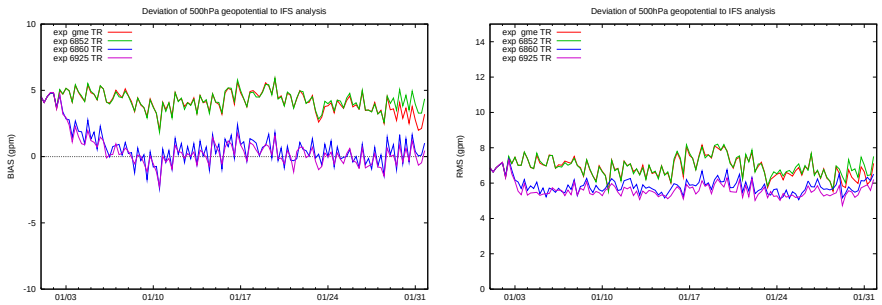

Figure 18: Comparison of the geopotential field at 500 hPa with IFS in the tropics: Time series of the bias (left) and the RMS (right) of analysis deviances of assimilation experiments w.r.t. IFS. Displayed are: Assimilation of IASI retrievals over sea only (pink), IASI retrievals over land and sea (blue), control experiment (green) and the operational assimilation of the GME (red)

2.7 Anomaly correlation coefficients

The anomaly correlation coefficients (ANOC) represents the correlation between the forecast and the analysis with respect to the model climate. The closer to value 1 the ANOC is, the better is the forecast when compared with a later analysis, and the better, in a common sense, is the forecast itself. The anomaly correlation coefficients of the two experiments with IASI radiances in comparison to the control experiment show a similar pattern for the three meteorological quantities geopotential at 500 hPa, temperature at 850 hPa, and pressure at mean sea level: In the northern hemisphere and in Europe, the impact of IASI observations is more or less neutral. A significant degradation of the ANOC can be seen in the tropics: Both experiments with IASI data result in a reduction of the ANOC by approximately 2-4%. In the southern hemisphere, the experiment 1 with assimilation of land IASI data is worse by about the same degree. The experiment 2 with assimilation of IASI radiances over sea only is close to the control, however still slightly worse. There is no apparent difference when comparing ANOC from 00 UTC and 12 UTC.

2.8 Conclusions of the impact experiment

The IASI level 2 product, containing retrievals of temperature and water vapour mixing ratio derived from IASI radiances, is experimentally studied for its use in a numerical weather prediction system. To this end, geopotential layer thickness observations are calculated from the level 2 data, and are assimilated into the global model GME with the three-dimensional variational assimilation scheme of the DWD. Only cloud-free IASI-observations are considered, and no bias correction is applied. If IASI retrievals over sea, land and sea-ice are assimilated, large drifts in the temperature field, especially in the higher latitudes, are obtained. The results are better for IASI observations over sea only. However, a distict vertically oscillating pattern of approximately 0.5 K is impressed on the tropical temperature field, visible in the bias and obviously correlated to the setup of the vertical partitioning of the thickness layers. The anomaly correlation coefficient, measuring the effect of the IASI observations on the quality of

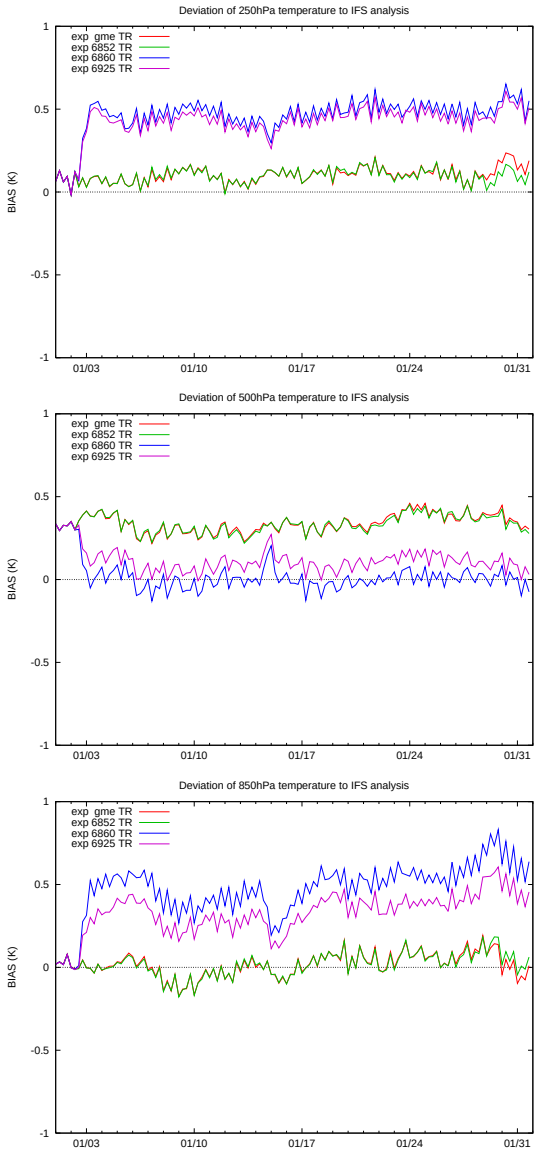

Figure 19: Comparison of the temperature fields with IFS in the tropics: Time series of the bias of analysis deviances of assimilation experiments w.r.t. IFS, at 250 hPa (top), 500 hPa (middle) and 850 hPa (bottom). Displayed are: Assimilation of IASI retrievals over sea only (pink), IASI retrievals over land and sea (blue), control experiment (green) and the operational assimilation of the GME (red)

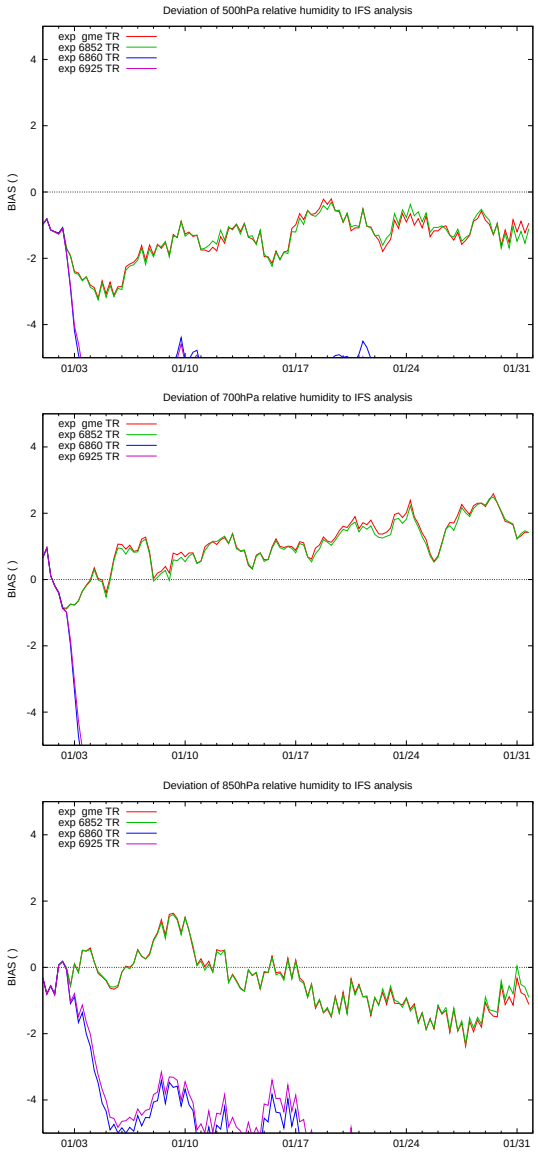

Figure 20: Comparison of the relative humidity fields with IFS in the tropics: Time series of the bias of analysis deviances of assimilation experiments w.r.t. IFS, at 500 hPa (top), 700 hPa (middle) and 850 hPa (bottom). Displayed are: Assimilation of IASI retrievals over sea only (pink), IASI retrievals over land and sea (blue), control experiment (green) and the operational assimilation of the GME (red)

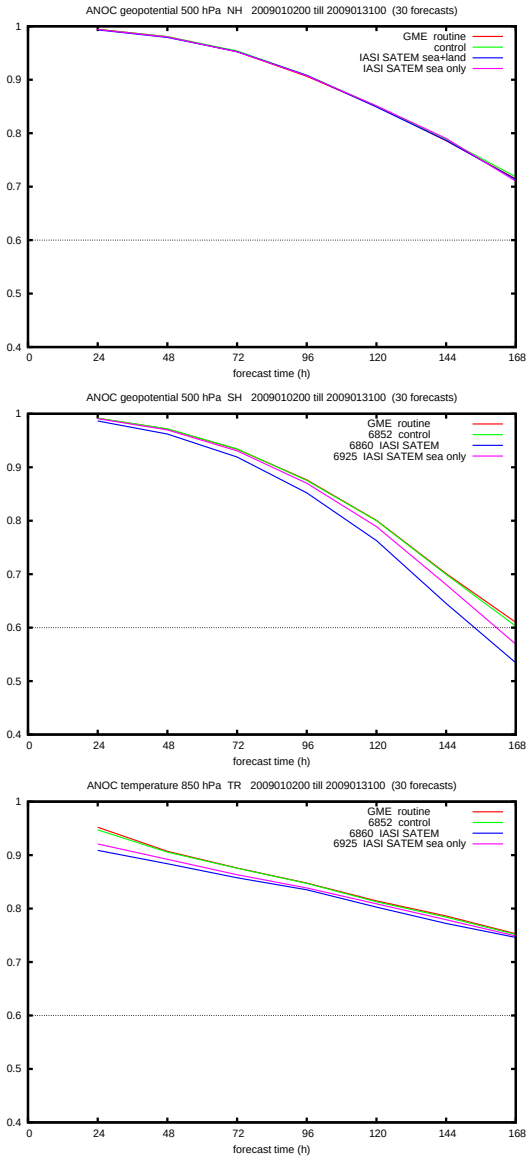

Figure 21: Anomaly correlation coefficients of the geopotential field at 500 hPa in the northern (top) and the southern (middle) hemisphere. The bottom figure shows the temperature field at 850 hPa in the tropics. Displayed are: Assimilation of IASI retrievals over sea only (pink), IASI retrievals over land and sea (blue), control experiment (green) and the operational assimilation of the GME (red)

the forecast, shows a more or less neutral impact in the northern hemisphere and a certain change to the worse in the other regions. Thus, the IASI level 2 data, processed in a way as it is done for this study, is not expected to improve the forecast when assimilated.

References

[1] A. P. McNally and P. D. Watts. A cloud detection algorithm for high-spectral-resolution infrared sounders. *Q.J.R. Meteorol. Soc.*, 129:3411, 2003.

[2] EUMETSAT: IASI Level 2 Product Guide
. http://oiswww.eumetsat.org/WEBOPS/eps-pg/IASI-L2/
/IASIL2-PG-4ProdOverview.htm, 7 Apr 2009.

[3] P. Schluessel, T. August, A. Arriaga, T. Hultberg, N. Pougatchev, P Bauer, and G. Radnoti. Generation and assimilation of IASI level II products. http://www.ecmwf.int/newsevents/meetings/workshops/2009/IASI_data/
/presentations/Schluessel.pdf, 2009.

[4] G. Kelly and J. Pailleux. Use of satellite vertical sounder data in the ECMWF analysis sytem. Technical memorandum 143, ECMWF, Reading, United Kingdom, 1988.